doi:10.1093/brain/awv263 BRAIN 2015: 138; 3238–3250 | 3238

BRAIN
A JOURNAL OF NEUROLOGY

Recessive mutations in *SLC13A5* result in a loss of citrate transport and cause neonatal epilepsy, developmental delay and teeth hypoplasia

Katia Hardies,[1,2] Carolien G. F. de Kovel,[3] Sarah Weckhuysen,[1,2,4] Bob Asselbergh,[5] Thomas Geuens,[2,6] Tine Deconinck,[1,2] Abdelkrim Azmi,[7] Patrick May,[8,9] Eva Brilstra,[3] Felicitas Becker,[10] Nina Barisic,[11] Dana Craiu,[12,13] Kees P. J. Braun,[3] Dennis Lal,[14] Holger Thiele,[14] Julian Schubert,[10] Yvonne Weber,[10] Ruben van 't Slot,[3] Peter Nürnberg,[14,15,16] Rudi Balling,[8] Vincent Timmerman,[2,6] Holger Lerche,[10] Stuart Maudsley,[2,7] Ingo Helbig,[17,18] Arvid Suls,[1,2] Bobby P. C. Koeleman[3] and Peter De Jonghe,[1,2,19] on behalf of the autosomal recessive working group of the EuroEPINOMICS RES Consortium[§]

[§]See Appendix 1.

The epileptic encephalopathies are a clinically and aetiologically heterogeneous subgroup of epilepsy syndromes. Most epileptic encephalopathies have a genetic cause and patients are often found to carry a heterozygous *de novo* mutation in one of the genes associated with the disease entity. Occasionally recessive mutations are identified: a recent publication described a distinct neonatal epileptic encephalopathy (MIM 615905) caused by autosomal recessive mutations in the *SLC13A5* gene. Here, we report eight additional patients belonging to four different families with autosomal recessive mutations in *SLC13A5*. *SLC13A5* encodes a high affinity sodium-dependent citrate transporter, which is expressed in the brain. Neurons are considered incapable of *de novo* synthesis of tricarboxylic acid cycle intermediates; therefore they rely on the uptake of intermediates, such as citrate, to maintain their energy status and neurotransmitter production. The effect of all seven identified mutations (two premature stops and five amino acid substitutions) was studied *in vitro*, using immunocytochemistry, selective western blot and mass spectrometry. We hereby demonstrate that cells expressing mutant sodium-dependent citrate transporter have a complete loss of citrate uptake due to various cellular loss-of-function mechanisms. In addition, we provide independent proof of the involvement of autosomal recessive *SLC13A5* mutations in the development of neonatal epileptic encephalopathies, and highlight teeth hypoplasia as a possible indicator for *SLC13A5* screening. All three patients who tried the ketogenic diet responded well to this treatment, and future studies will allow us to ascertain whether this is a recurrent feature in this severe disorder.

1 Neurogenetics Group, VIB-Department of Molecular Genetics, University of Antwerp, Antwerp, Belgium
2 Laboratory of Neurogenetics, Institute Born-Bunge, University of Antwerp, Antwerp, Belgium
3 Departments of Medical Genetics and Child Neurology, University Medical Center Utrecht, Utrecht, The Netherlands
4 Inserm U 1127, CNRS UMR 7225, Sorbonne Universités, UPMC Univ Paris 06 UMR S 1127, Institut du Cerveau et de la Moelle épinière, ICM, Centre de reference épilepsies rares, Epilepsy unit, AP-HP Groupe hospitalier Pitié-Salpêtrière, Paris, France
5 VIB-Department of Molecular Genetics, University of Antwerp, Antwerp, Belgium
6 Peripheral Neuropathy Group, VIB-Department of Molecular Genetics, University of Antwerp, Antwerp, Belgium
7 Translational Neurobiology Group, VIB-Department of Molecular Genetics, University of Antwerp, Antwerp, Belgium
8 Luxembourg Centre for Systems Biomedicine, University of Luxembourg, Luxembourg
9 Institute for Systems Biology, Seattle, USA

Received April 30, 2015. Revised June 19, 2015. Accepted July 7, 2015. Advance Access publication September 18, 2015

10 Department of Neurology and Epileptology, Hertie Institute for Clinical Brain Research, Eberhard-Karls University, Tübingen, Germany
11 Division for Child Neurology, Department of Pediatrics, Clinical Medical Centre Zagreb, University of Zagreb Medical School, Zagreb, Croatia
12 Pediatric Neurology Clinic Al Obregia Hospital, Bucharest, Romania
13 Carol Davila University of Medicine and Pharmacy, Bucharest, Romania
14 Cologne Center for Genomics (CCG), University of Cologne, Cologne, Germany
15 Center for Molecular Medicine Cologne (CMMC), University of Cologne, Cologne, Germany
16 Cologne Excellence Cluster on Cellular Stress Responses in Aging-Associated Diseases (CECAD), University of Cologne, Cologne, Germany
17 Department of Neuropediatrics, University Medical Center Schleswig-Holstein, Christian Albrechts University, Kiel, Germany
18 Division of Neurology, The Children's Hospital of Philadelphia, Philadephia, USA
19 Division of Neurology, Antwerp University Hospital, Antwerp, Belgium

Correspondence to: Prof. Dr Peter De Jonghe,
Neurogenetics Group,
VIB-Department of Molecular Genetics,
University of Antwerp – CDE (Building V),
Antwerp,
Belgium
E-mail: peter.dejonghe@molgen.vib-ua.be

Keywords: recessive disorder; epileptic encephalopathy; teeth hypoplasia; SLC13A5; NaCT; anaplerosis

Abbreviation: NaCT = sodium-dependent citrate transporter

Introduction

The epileptic encephalopathies are a clinically and aetiologically heterogeneous subgroup of epilepsy syndromes. Starting at an early age, patients with an epileptic encephalopathy have recurrent and mostly pharmaco-resistant seizures, leading to different degrees of developmental delay. In addition, patients often present variable (non-) neurological comorbidities. Based on the age at seizure onset, seizure type(s), brain MRI features, EEG patterns and disease course, distinct electroclinical syndromes can be defined within the group of epileptic encephalopathies (Berg *et al.*, 2010). All epileptic encephalopathies are rare disorders; depending on the specific phenotype incidences range from 1/10 000 to 1/1 000 000 per live birth. Epidemiological studies, however, do indicate that all epileptic encephalopathies together constitute almost 25% of the childhood epilepsies (Kramer *et al.*, 1998; Panayiotopoulos, 2005).

Due to the severe phenotype, patients with an epileptic encephalopathy present mostly as isolated cases. An underlying metabolic or structural abnormality can be identified in some, but most patients are thought to carry a genetic defect (Claes *et al.*, 2001; Weckhuysen and Korff, 2014). Both heterozygous *de novo* single nucleotide variants and structural rearrangements have been shown to contribute to the aetiology of epileptic encephalopathies in these isolated patients (Mefford *et al.*, 2011; Allen *et al.*, 2013; Veeramah *et al.*, 2013). Exceptionally, two or more siblings are affected with an epileptic encephalopathy and for some of these families a somatic or germline mosaicism can be identified. Nevertheless, recessive gene defects have also been reported, mainly but not exclusively, in consanguineous families (Gennaro *et al.*, 2006; Molinari *et al.*, 2009; Paciorkowski *et al.*, 2013).

Recently, three families encompassing a total of seven individuals with a distinct neonatal onset epileptic encephalopathy (MIM 615905) were found to carry compound heterozygous or homozygous missense mutations in the *SLC13A5* gene (Thevenon *et al.*, 2014). *SLC13A5* encodes a high affinity sodium-dependent citrate transporter (NaCT). The effect of these mutations was not studied *in vitro* or *in vivo*, but a disruption of sodium binding capacity was suggested to cause a loss of citrate transport. Here, we report four additional families with neonatal epileptic encephalopathy caused by autosomal recessively inherited *SLC13A5* mutations, and identify teeth hypoplasia as a distinctive feature of the *SLC13A5* encephalopathy. We furthermore investigated the impact of the identified variants on protein expression, cellular localization and citrate transport capacity.

Materials and methods

This study is the result of a combined effort of different European research groups working on familial forms of epileptic encephalopathies. Studies were approved by the Ethical Committees of the respective local institutions. Parents or legal guardians of each patient signed an informed consent form for participation.

Massive parallel sequencing and data analyses

Three families with siblings presenting an epileptic encephalopathy phenotype were included in separate massive parallel sequencing studies (Fig. 1). Family A is a consanguineous Dutch family with two affected half-brothers and three healthy sisters: both mothers were cousins and related to the common father. Whole exome sequencing was performed on DNA of the two mothers, the father and one of the affected boys. Insufficient DNA was available to include the deceased half-brother in the massive parallel sequencing analysis. The exome was enriched with the SureSelect® Human 35 Mb capturing kit (Agilent) and sequenced on a SOLiD™ 4 System (Applied Biosystems). Reads were aligned with the Burrows-Wheeler Aligner (Li and Durbin, 2009). Variant calling and analysis was done with a custom pipeline. Parents and all three affected children of the German Family C were also subjected to whole-exome sequencing, using sequencing procedures as previously described by Reinthaler *et al.* (2015). In brief, DNA was fragmented using sonification technology (Covaris). Fragments were end repaired, adaptor ligated and enriched with the SeqCap EZ Human Exome Library® v2.0 (Roche NimbleGen) before analysis on the Illumina HiSeq 2000® sequencer. Scripts developed in-house at the Cologne Center for Genomics (Cologne, Germany) were applied to detect protein changes, affected splice sites, and overlaps with known disease genes. Whole-genome sequencing was performed by Complete Genomics on DNA of both healthy parents and the two affected children of the non-consanguineous Croatian Family B. Their service includes library preparation, massively parallel short-read sequence by ligation, sequence mapping, local *de novo* assembly, as well as structural variant calling and generation of alignment and coverage files (Drmanac *et al.*, 2010). All variants were annotated and analysed with the in-house developed GenomeComb tool (Reumers *et al.*, 2012).

Variant prioritization was standardized between all three pipelines as previously described (Hardies *et al.*, 2014; Schubert *et al.*, 2014). In short, variants were selected based on the following criteria: (i) high quality calls (i.e. coverage $\geqslant 10$ and exclusion of repeat regions); (ii) absent in a homozygous state and frequency below 1% in control populations [data from 1000Genomes, Exome Variant Server (EVS), Exome Aggregation Consortium, and in-house projects]; (iii) predicted impact on the encoded protein (i.e. missense, nonsense, frameshift and essential splice variants) according to the RefGene annotation hg19; and (iv) segregation analysis fitting an autosomal recessive model (i.e. homozygous or compound heterozygous). In addition, heterozygous variants called in both siblings and absent in the parents were selected under a parental mosaicism hypothesis. Candidate variants were validated using direct Sanger sequencing in the respective families, including all available relatives (Supplementary Table 1).

Genetic follow-up study

As clinically matched follow-up cohort, 77 patients with a history of epilepsy and developmental delay combined with either a neonatal seizure onset ($n = 61$) and/or a possible recessive inheritance based on the presence of consanguinity or multiple affected siblings ($n = 20$) were selected for direct Sanger sequencing of the candidate gene. All coding and untranslated regions of *SLC13A5* were PCR amplified using standard procedures. Primers were designed flanking at least 50 bp away from exon–intron boundaries (available on request). Separation of PCR fragments was done on an ABI3730 automated sequencer (Applied Biosystems).

Protein predictions

Six species-specific NaCT proteins were aligned using the ClustalW2 Multiple Sequence Alignment of EMBL-EBI (Larkin *et al.*, 2007) to determine amino acid conservation. Folding of the human NaCT protein was predicted with the Phyre2 server (Kelley and Sternberg, 2009). The FoldX plugin for YASARA was used for visualization and interpretation of protein stability (Van Durme *et al.*, 2011).

Plasmid generation

Full-length human *SLC13A5* cDNA (BC104795) was PCR-amplified from the I.M.A.G.E Consortium Clone ID 8143798 (http://image.llnl.gov; Source BioScience LifeSciences) (Lennon *et al.*, 1996). The N-terminal V5-label was added by PCR primer extension. All plasmids were generated using the Gateway® Cloning Technology according to the manufacturer's instructions (Life Technologies) using the pDONR221 as entry clone. Identified single nucleotide variants were introduced into the wild-type plasmid by site-directed mutagenesis (Zheng *et al.*, 2004), whereas the 11 bp duplication (CAGGAGAAAGT) was embedded by overlapping PCR. The different entry clones were subcloned into the pLENTI6-DEST expression vector for lentiviral transduction. In addition to the V5 containing plasmid, the wild-type construct was also subcloned into an enhanced green fluorescent protein (eGFP) containing destination vector. All templates were verified by direct Sanger sequencing.

Cell culture and treatment conditions

All experiments were performed in human embryonic kidney (HEK293T) cells, which were continuously kept at 37°C in a humidified atmosphere with 5% CO_2. Cells were cultured in Dulbecco's Modified Eagle Medium (DMEM), high glucose (Gibco®) enriched with 10% heat-inactivated foetal calf serum, 1% L-glutamine, 1% penicillin-streptomycin and 1% sodium pyruvate (all obtained from Life Technologies). Stable cell lines were kept under selection by adding 3 µg/ml of Blasticidin (InvivoGen) to the culture medium.

To inhibit proteasome function, 2×10^6 cells were seeded in 100-mm diameter cell culture dishes and treated the next day with 10 µM MG-132 (Merck Chemicals) or with an equal volume of the solvent (dimethyl sulphoxide; DMSO). Cells were harvested after 8 h and pelleted by centrifugation for western blot analysis. To induce endoplasmic reticulum stress cells were treated with 1 µg/ml tunicamycin (Sigma-Aldrich) for 6 h before collection.

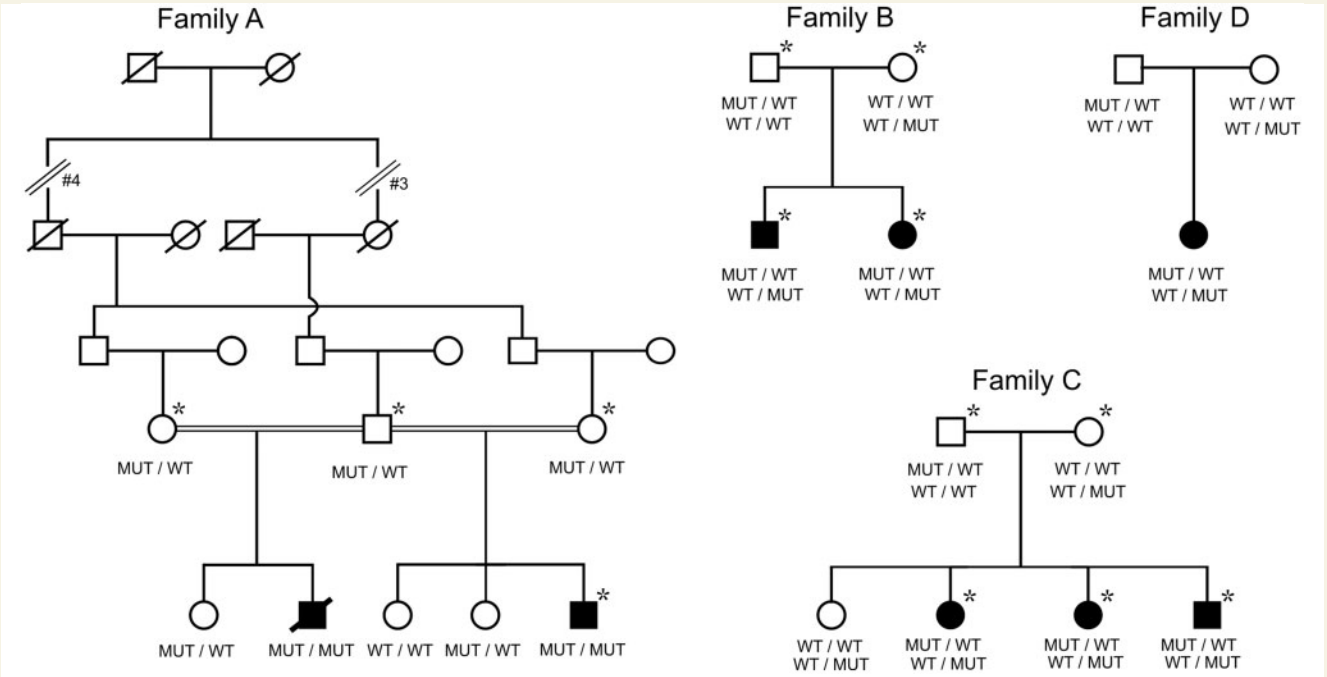

Figure 1 Pedigrees of the four families with autosomal recessive *SLC13A5* mutations described in this study. Coloured individuals are diagnosed with epileptic encephalopathy. Hask symbol refers to number of generations not shown in the figure, and asterisk refers to the individuals subjected to massive parallel sequencing. MUT = mutation; WT = wild-type. Heterozygous carriers are thus depicted as MUT/WT, compound heterozygous individuals as MUT/WT and WT/MUT (reflecting two different heterozygous variants one on each allele), and homozygous mutation carriers as MUT/MUT.

RNA extraction and quantitative PCR

According to manufacturer's instructions, RNA was extracted with the RNeasy® Mini Kit (Qiagen) from 5×10^6 pelleted HEK293T cells transduced with the respective plasmids. The extracted RNA was further treated with the TURBO DNA-free™ Kit (Ambion) and converted to cDNA using the SuperScript® III First-Strand Synthesis System (Life Technologies) with both oligo-dT and random hexamer primers. RNA and cDNA concentrations were measured with the NanoDrop1000 (Thermo Scientific). Endogenous expression of all five SLC13A protein family members was verified by PCR amplification of 20 ng cDNA with specific exon-spanning primers. Verification of plasmid expression was performed with quantitative PCR on 10 ng cDNA, using a Fast SYBR® Green master mix (Life Technologies) with primer pairs specific for *SLC13A5* and five housekeeping genes: resultant data were analysed with the ViiATM7 PCR system (Life Technologies). Measurements were normalized against the two most stable housekeeping genes with geNorm (Vandesompele *et al.*, 2002).

Western blot

Pelleted HEK293T cells expressing the respective proteins were homogenized in lysis buffer [150 mM NaCl, 0.5% sodium deoxycholate, 1% sodium dodecyl sulphate (SDS), 1% NP-40, 50 mM Tris-HCl pH 7.4] supplemented with protease inhibitors (Roche Diagnostics-Applied Science). Concentrations of the supernatant protein were determined using a Pierce™ BCA Protein Assay Kit (Thermo Scientific). Equal amounts of protein (20 µg) were diluted in 4× NuPAGE® LDS Sample buffer and denatured for 30 min at 37°C. Subsequent size-separation was performed with SDS-polyacrylamide gel electrophoresis on NuPAGE® Novex® 4–12% Bis-Tris gels, which were later electrotransferred to a nitrocellulose membrane (GE Healthcare Lifescience). Primary antibody anti-V5 (1:2000; Life Technologies R960-25) was incubated overnight at 4°C. Intermediate washings steps were done with PBS/0.1%Tween-20. Secondary anti-mouse IgG2a horseradish peroxidase was diluted 1:5000 (Jackson Immuno Research Laboratories Inc.) and incubated for 1 h at room temperature. Visualization was effected with enhanced chemiluminescence detection (Pierce® ECL Plus Western Blotting Substrate, Thermo Scientific) using an ImageQuant™ LAS4000 system (GE Healthcare Life Sciences). Antibodies against CHOP, Bip, eIF2a, and phospho-eIF2a were used as downstream protein markers for endoplasmic reticulum stress (all acquired from Cell Signaling Technologies and diluted at 1:1000 for overnight incubation at 4°C). Finally, as an equal loading control, every membrane was reincubated with primary antibody (1:5000) for 1 h at room temperature against either α-tubulin (ab4074) or β-actin (A5441).

Cell staining, microscopy and image analysis

To visualize localization of wild-type NaCT at the plasma membrane, cells expressing wild-type C-terminal eGFP-labelled

SLC13A5 were seeded in live cell imaging dishes. After 24 h, these cells were incubated for 10 min at 37°C with 5 µg/ml fluorescently-labelled wheat germ agglutinin (WGA-Alexa Fluor 555 conjugate; Life Technologies) and immediately imaged with a confocal microscope. For immunofluorescence staining, 5×10^4 cells expressing N-terminal V5 labelled wild-type or mutant *SLC13A5* were seeded on 12 mm diameter cover slips and 48 h later fixed with 4% paraformaldehyde for 20 min at room temperature. Cells were permeabilized with 0.5% Triton™ X-100 for 2 min, blocked with 2% bovine serum albumin for 1 h and sequentially incubated overnight at 4°C with primary antibodies against the *SLC13A5* encoded NaCT protein (1:250; Abcam ab89181) and against the endoplasmic reticulum (anti-KDEL, 1:250; Enzo Life Sciences 10C3). With intermediate phosphate-buffered saline washing steps, the secondary antibodies goat anti-mouse IgG1 Alexa Fluor® 488 and goat anti-mouse IgG2a Alexa Fluor® 633 (both 1:500; Life Technologies) were sequentially added for 1 h at room temperature. Nuclei were stained for 10 min with 1:20 000 Hoechst 33342 (Life Technologies). Coverslips were mounted (Dako) and images (1036 × 1036 pixels; pixel size 98 nm × 98 nm) were taken with a Zeiss LSM700 confocal microscope using a ×63/1.40 plan-apochromatic objective. Possible cross-talk of the fluorescence channels was excluded by using frame-by-frame scanning.

To determine the amount of NaCT maintained in the endoplasmic reticulum (co-localization with KDEL) an image analysis pipeline was established using the CellProfiler software (Kamentsky *et al.*, 2011). In brief: raw Zeiss LSM files were loaded, primary object detection of the nuclei (Otsu global thresholding method) was followed by secondary object detection of the cells (propagation method using Otsu global thresholding in the KDEL channel), and tertiary object detection (based on the previously identified objects) to obtain the cytoplasmic outline of each cell. In the resulting cytoplasmic regions, the correlation of pixel intensities between the NaCT and KDEL channels was measured (i.e. the Pearson's correlation coefficient). To exclude individual cells not expressing the NaCT construct, a fixed cut-off value (>0.3) was set for the mean intensity of the NaCT channel in the cytoplasmic domain. For each genotype between 92 and 451 cells were measured.

Cell feeding experiment and mass spectrometry

^{13}C-labelled citrate (citric acid-2,4-$^{13}C_2$) was obtained from Sigma-Aldrich (Belgium). Cells expressing the respective proteins (2×10^6) were seeded in 100-mm diameter dishes and 48 h later incubated with uptake buffer (140 mM NaCl, 5.4 mM KCl, 1.8 mM $CaCl_2$, 0.8 mM $MgSO_4$, 5 mM D-glucose, and 25 mM HEPES-Tris; pH 7.4), supplemented with 200 µM ^{13}C-labelled citrate for 4 h at 37°C. Cells were extensively washed with uptake buffer, counted, and pelleted. To study the effect of lithium on citrate transport efficiency, the NaCl concentration in the uptake buffer was partially replaced with LiCl (10 mM). Pellets were extracted in acidified methanol (0.05 M HCl). After centrifugation the supernatants were dried under nitrogen flux and derivatized with diazomethane. Methylated ^{13}C-labelled citrate was measured using an electrospray ACQUITY TQD UPLC-MS/MS device (Waters) by injecting 6 µl and separation in an ACQUITY UPLC BEH C18 column (1.7 × 2.1 × 100 mm). Calibration curves were generated by running standards under the optimized mass spectrometric conditions. Based on specific diagnostic transition (m/z of 237>145), the ESI(+) multiple reaction monitoring mode was used for quantification of the methylated ^{13}C-labelled citrate. Chromatograms were processed using the Masslynx software V4.1 (Waters) and interpolated against the external calibration curve.

Results

Identification of autosomal recessive *SLC13A5* mutations

Using the described filtering strategies whole-exome sequencing revealed two homozygous missense variants in the affected child of Family A: one in *SLC13A5* and one in *KCNAB3*. His deceased half-brother was also found to carry both mutations in a homozygous state after direct Sanger sequencing of the mutated regions. Whole-genome sequencing identified compound heterozygous variants in *FAT2* (two amino acid substitutions) and *SLC13A5* (two premature stops) in both affected children of Family B, whereas compound heterozygous missense variants in *SLC13A5* were identified in all three affected children of Family C by whole-exome sequencing. Based on the full segregation pattern in all available family members (Fig. 1), frequency of the candidate variants in the control populations, prediction programs, the overlapping genetic data and clinical phenotype of the patients, the variants in *SLC13A5* were considered pathogenic in all three families (Supplementary Table 1). Direct Sanger sequencing of 77 additional index cases with neonatal epileptic encephalopathy and/or a presumed autosomal recessive inheritance pattern led to the identification of two *SLC13A5* missense mutations in the only child of Family D. Family D is Romanian, hence all the identified *SLC13A5* mutation carriers are of European ethnicity.

Altogether we identified seven different autosomal recessive inherited variants in *SLC13A5* in four independent families of European origin (Table 1). Five resulted in an amino acid substitution and two introduced a premature stop codon. Two of the missense variants (p.Gly219Arg; p.Thr227Met) have previously been reported in a compound heterozygous state in two independent families with neonatal epileptic encephalopathy (Thevenon *et al.*, 2014). The nonsense variant (p.Trp341*) was found in 1/6502 (0.015%) individuals reported in the EVS; four of the missense variants were reported in the ExAC browser whereas the frame shift (p.Pro407Arg*fs**12) and last missense variant (p.Asp524His) were novel. None of the variants have been observed in a homozygous state. The identified carrier rate is compatible with the prevalence of neonatal epileptic encephalopathy and the autosomal recessive inheritance pattern. Other naturally occurring variants

Table 1 Overview of *SLC13A5* mutations associated with epileptic encephalopathy

Family	cDNA change	Protein change	Mutation type	Carrier frequency
Current report				
A	c.1280C>T	p.Ser427Leu	Missense	rs548065551 - 0.002%
B	c.1022G>A	p.Trp341*	Nonsense	rs150203483 - 0.015%
	c.1207_1217dup11	p.Pro407Arg*fs**12	Frameshift	-
C	c.425C>T	p.Thr142Met	Missense	0.002%
	c.655G>A	*p.Gly219Arg*	Missense	rs144332569 - 0.041%
D	*c.680C>T*	*p.Thr227Met*	Missense	0.005%
	c.1570G>C	p.Asp524His	Missense	-
Reported by Thevenon *et al.*, 2014				
1	*c.655G>A*	*p.Gly219Arg*	Missense	rs144332569 - 0.041%
	c.680C>T	*p.Thr227Met*	Missense	0.005%
2	c.1463T>C	p.Leu488Pro	Missense	-
3	*c.655G>A*	*p.Gly219Arg*	Missense	rs144332569 - 0.041%
	c.680C>T	*p.Thr227Met*	Missense	0.005%

Reference sequence NM_177550.4 (hg19) was used for cDNA and NP_808218.1 for protein changes. Patients of Family A identified here and Family 2 reported previously, were homozygous for the respective mutation. All other patients inherited a heterozygous mutation from their father, and another from their mother. Mutations in italic were identified in both studies. Carrier frequencies were obtained from the EVS and ExAC browser.

in *SLC13A5* are also rare, i.e. only 36 non-synonymous variants have been reported in EVS and 215 in the ExAC browser, with only one exceeding an allele frequency of 0.02% and most only seen once.

Clinical features of patients with autosomal recessive *SLC13A5* mutations

Clinical details are summarized in Supplementary Table 2. In short, all eight patients reported here had focal clonic seizures on the first day of life. Early in the course of their disease, status epilepticus (hemiconvulsive, convulsive and non-convulsive) was frequent: 7/8 patients. Although multiple seizure types occurred later in life, all patients had prominent convulsive seizures (hemiconvulsions of changing sides and/or generalized tonic-clonic seizures) with frequent fever-sensitivity (6/8 patients). Seizure outcome varied from multiple seizures weekly despite treatment ($n = 5$) or even death due to status epilepticus ($n = 1$), to seizure freedom between the age of 3 and 7 years ($n = 2$) without anti-epileptic drugs. Interictal EEG showed multifocal or shifting focal abnormalities in all patients, except for one whose EEG was always normal (Patient 1, Family C). Epileptic abnormalities on EEGs at onset were predominantly seen in posterior areas [as demonstrated by Thevenon *et al.* (2014)] in 3/5 patients for whom EEGs could be reviewed. At a later age, no predilection for a specific brain area was seen. Ictal EEG at onset was only available for one patient and showed generalized epileptic discharges during a myoclonic seizure. Both sibs of Family A had periventricular leukomalacia-like abnormalities on brain MRI with increased lactate on magnetic resonance spectroscopy in one (spectroscopy was not performed in other patients). Three patients with treatment-resistant seizures initiated ketogenic diet after failure of multiple anti-epileptic drug trials. All three patients responded well, but had to stop the diet eventually due to gastrointestinal side effects or problems with compliance. Neurological examination revealed a developmental outcome ranging from mild to severe intellectual disability, plus variable combinations and degrees of ataxia, choreoathetosis, spasticity and microcephaly. Three of the seven children for whom growth parameters were available were underweight or thin. Interestingly, all of our patients were noted to have teeth hypoplasia and/or hypodontia (Fig. 2), which was also described in three of the previously reported *SLC13A5* patients. This clinical feature was identified either by a medical geneticist, a neurologist or a dentist.

PCR for verification of SLC13A expression

To evaluate the functional consequences of the identified variants, we generated HEK293T cell lines ectopically expressing wild-type or mutant *SLC13A5*. To confirm successful transduction of the *SLC13A5* plasmids a quantitative PCR experiment on cDNA converted from cell extracted mRNA was performed. All wild-type and mutant cell lines had an increased *SLC13A5* expression (data not shown). With a standard PCR amplification we also determined endogenous expression of two *SLC13A2* isoforms (NM_003984.3 and NM_001145975.1), one *SLC13A4* isoform (NM_012450.2) and negligible levels of *SLC13A5* (NM_177550.4) in the HEK293T cell background (Supplementary Fig. 3).

Western blot for verification of plasmid translation

Western blotting on whole cell lysates from HEK293T cells expressing V5-labelled wild-type human *SLC13A5* cDNA

Figure 2 Illustrative pictures of hypodontia in patients with *SLC13A5* mutations. Patients 1 and 2 of Family B.

(NP_808218.1) resulted in a specific band pattern consisting of a primary band, a lower secondary band (Fig. 3A) and four tertiary products. This pattern suggested the presence of incompletely folded or unassembled proteins and probably post-translational processing of the wild-type protein. Based on the wild-type pattern, we further distinguished two different categories of mutant cell lines (further referred to as mutation type I and II). In mutation type I, cells express variants leading only to the formation of a single protein band. These include two of the substitutions p.Ser427Leu and p.Gly219Arg, which form a protein band corresponding to the secondary wild-type band; and both premature stop variants p.Trp341* and p.Pro407Arg*fs**12, which form truncated proteins of the expected size. In mutation type II, cells express variants leading to a similar pattern as the wild-type. These are the remaining three substitutions: p.Thr227Met, p.Asp524His, and p.Thr142Met.

Stimulation with the proteasome inhibitor, MG-132, resulted in an upregulation of the truncated proteins encoded by mutations introducing a premature stop. The expression of wild-type and the five other mutant proteins was also increased but to a much smaller extent (Supplementary material). Blockage of N-linked glycosylation with tunicamycin resulted in the irregular detection of downstream endoplasmic reticulum-stress markers. The wild-type expressing cells showed no induction of endoplasmic reticulum stress, whereas an inconsistent upregulation of phospho-eIF2a and/or CHOP was seen for all mutants in separate experiments (data not shown).

Wild-type and mutation type II proteins localize at the plasma membrane

In cells expressing wild-type *SLC13A5* the bulk of the protein is present at the plasma membrane, which was shown by immunostaining with a NaCT-specific antibody (Fig. 3B). This expected localization of NaCT was further confirmed by expressing eGFP-fused NaCT, which co-localized with the plasma membrane marker WGA (Supplementary material). A similar staining pattern at the plasma membrane was observed for cells expressing mutation type II variants. In contrast, mutation type I proteins could not be detected at the plasma membrane and were only present in the endoplasmic reticulum as shown by an almost complete overlap with the endoplasmic reticulum marker KDEL (Fig. 3B and Supplementary Fig. 6). To objectively quantify the amount of co-localization between NaCT and the endoplasmic reticulum for the different genotypes, we measured the Pearson's correlation of the two fluorescent channels in the cytoplasmic region of a high number of cells. We found a much higher co-localization between mutation type I NaCT proteins and the endoplasmic reticulum compared to mutation type II and wild-type proteins (Fig. 3C). We were unable to visualize endogenous expression of the protein in non-transduced cells.

Both mutation types cause a loss of citrate transport

Upon stimulation with a physiological buffer containing ^{13}C-labelled citrate, we measured a small amount of ^{13}C-citrate in the extracted content of cells expressing wild-type NaCT (on average 1.13 nM/million cells), supporting the presence of a functional citrate transporter on the plasma membrane (Supplementary Fig. 7). Despite the plasma membrane localization of mutation type II NaCT proteins, none of the mutant cell lines were found to take up measurable amounts of ^{13}C-citrate from the extracellular medium. The levels of endogenous citrate were comparable between all cell lines (including the non-transduced control), indicating viable and healthy HEK293T cells. Cells expressing the N-terminal V5- or C-terminal GFP-tagged wild-type NaCT proteins showed comparable

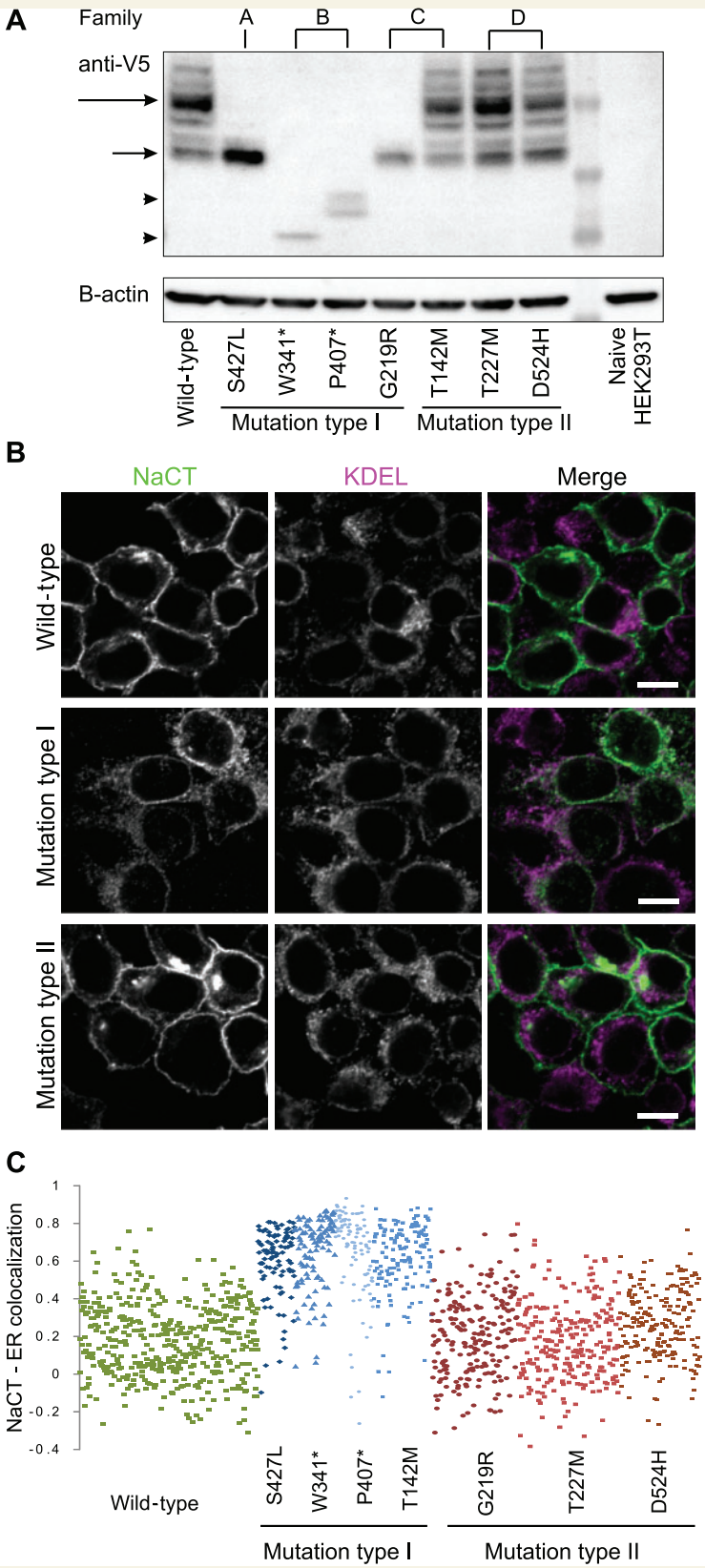

Figure 3 Protein translation and localization of *SLC13A5* in HEK293T cells. (**A**) Western blot of whole cell lysates shows multiple protein bands resulting from the translation of wild-type *SLC13A5* plasmid. Primary and secondary bands are indicated with a long and shorter arrow, respectively. Western blot of whole cell lysates expressing the missense mutation identified in Family A, and one of the missense mutations identified in Family C (mutation type I) show only the secondary band. Both premature stop mutations identified in Family B lead to the formation of an aberrant protein (indicated with arrowheads). The three remaining missense variants, found in Family C and D, (mutation type II) show a

(continued)

measurements, excluding a significant interference of the labels. Adding lithium to the uptake buffer did not enhance the uptake of ^{13}C-labelled citrate.

Protein predictions

Sequence alignment indicated a high conservation of the NaCT orthologues throughout evolution (Supplementary material). Based on the domain annotations reported by Mancusso *et al.* (2012), the amino acid changes introduced by the *SLC13A5* missense variants are located in highly conserved transmembrane (TM) domains or binding sides: p.Ser427Leu in TM9b, p.Gly219Arg in TM5a, p.Thr142Met near the first sodium-binding site, p.Thr227Met in TM5b, and p.Asp524His in TM11. The nonsense and frame shift variants introduce a premature stop codon in the loop between TM7 and TM8, and in TM9, respectively. For 3D modelling, the Phyre2 prediction tool primarily used the crystal structure of the bacterial sodium-dependent dicarboxylate transporter (VcIndy: 10.2210/pdb4f35) (Mancusso *et al.*, 2012). Four hundred and thirty-seven residues or, 77% of the human protein, was modelled at >90% accuracy. Stability of the mutant proteins was estimated based on alterations in free energy change (ddG) and Van der Waals (VdW) forces induced by the amino acid substitutions. Two mutants, p.Gly219Arg and p.Asp524His, were predicted to have a destabilizing effect on the protein with an average ddG of 22.26 and 1.94 kcal/mol, respectively. The two mutation type I substitutions (p.Ser427Leu and p.Gly219Arg) were furthermore predicted to cause VdW clashes. The location of mutation type II substitutions was visualized in a 3D model of the protein. Two of the mutations type II variants are clearly located in the predicted citrate binding pocket (Fig. 4).

Discussion

Epileptic encephalopathies are a clinically and genetically heterogeneous subgroup of the epilepsies. Although most patients are thought to carry heterozygous *de novo* mutations, autosomal recessive inherited mutations have to be considered, especially in families with multiple affected siblings. A recent study illustrated this with the identification of autosomal recessive mutations in *SLC13A5* in three families, including a total of seven patients with a distinct neonatal epileptic encephalopathy (MIM 615905) (Thevenon *et al.*, 2014). By describing eight additional

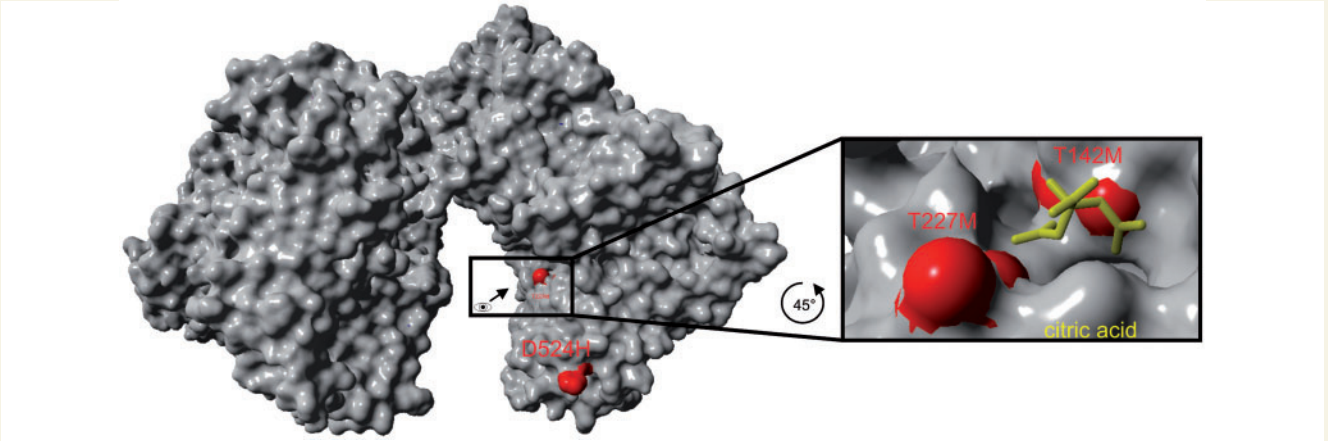

Figure 4 3D modelling. The crystal structure of the bacterial sodium-dependent dicarboxylate transporter (pdb4f35) was imported in YASARA as a dimer. Based on the protein sequence alignment (Supplementary material) we visualized the amino acids corresponding with the location of the three mutation type II substitutions (red). p.Thr142Met and p.Thr227Met shown in the inset are clearly located inside the citrate binding pocket (citric acid in yellow), whereas p.Asp524His (transmembrane domain 11) is located at the periphery.

Figure 3 Continued

similar protein pattern as the wild-type. β-Actin staining confirmed equal loading and the clear background in non-transduced HEK293T supports specific binding of the anti-V5 antibody. Shifts in band intensity are likely due to differences in cell transduction efficiency and growth selection. The SeeBlue® Plus2 Pre-stained Protein Standard was used as size indicator. (**B**) Immunocytochemistry was performed on all cell lines with an antibody against NaCT and KDEL (endoplasmic reticulum marker). Example images of all cell lines can be found in the Supplementary material. In wild-type NaCT-expressing cells and in mutation type II expressing cells NaCT is mainly present at the plasma membrane, while cells expressing mutation type I variants have a complete absence of NaCT on the plasma membrane and the detected proteins mainly co-localize with the endoplasmic reticulum. Scale bar = 10 μm. (**C**) Plot of the Pearson's correlation coefficient between NaCT and KDEL fluorescence channels for all eight cell lines. The higher the correlation value (*y*-axis), the higher the co-localization of NaCT with the endoplasmic reticulum. Each dot represents an individual cell measurement: wild-type is shown in green, mutation type I in blue, and mutation type II in red.

patients—belonging to four different families—carrying autosomal recessive inherited mutations in *SLC13A5*, we establish independent proof of a causal relationship with a distinct epileptic encephalopathy phenotype. We confirm the clinical hallmarks of seizure onset during the first days of life, progression to refractory epilepsy with frequent status epilepticus early in life, and following developmental delay. The presence of neonatal clonic seizures and prominent convulsive seizures (hemiconvulsions of changing sides and/or generalized tonic-clonic seizures) later in life distinguishes these patients from the most frequent genetic neonatal epileptic encephalopathies, *KCNQ2* and *STXBP1* encephalopathy, where tonic seizures and infantile spasms predominate. In addition, a high fever sensitivity is often noted and whereas all patients reported by Thevenon *et al.* (2014) had severe to profound developmental delay, cognitive outcome seems to be variable and ranges from mild to profound in the patients described here. Description of additional patients will tell whether this clinical variability is related to the *SLC13A5* defect (e.g. by an increased vulnerability to ischaemia) or additional (genetic) factors play a role (e.g. the *KCNB3* variant of which the impact remains to be determined). We also underline that all of our patients—and three of the patients reported in literature—have noticeable teeth hypoplasia or hypodontia (Fig. 2). We believe that this clinical feature can be an indicator for *SLC13A5* encephalopathy and should warrant *SLC13A5* screening.

We identified seven autosomal recessive mutations in *SLC13A5*: five amino acid substitutions and two premature stops. Based on protein formation and localization, we distinguished two mutation types (I and II). For two of the amino acid substitutions and both premature stops (mutation type I), we found a loss of correctly formed NaCT protein and subsequent loss of plasma membrane localization; all the mutant type I proteins were retained in the endoplasmic reticulum (p.Trp341*, p.Pro407Arg*fs**12 and p.Ser427Leu, p.Gly219Arg). For the two premature stops it should be noted that by transducing pre-spliced and full-length cDNA in our experiments, we circumvent the natural mechanism of nonsense-mediated mRNA decay. Although the observed truncated proteins might thus be absent in a natural system, the overall outcome (i.e. lack of correct NaCT formation and plasma membrane localization) is the same. Protein formation and localization for the mutation type II substitutions (p.Thr227Met, p.Asp524His and p.Thr142Met) was similar to the wild-type. A possible explanation for the difference in protein processing between the two types of missense mutations within the same cell system could lie in the nature of the amino acid substitution: mutation type I variants cause a shift in polarity/hydrophobicity, whereas mutation type II variants do not (Supplementary Fig. 9). This is also supported by the predicted VdW clash induced by the mutation type I substitutions and the enormous change in free energy for at least one of them (p.Gly219Arg: 22.26 kcal/mol).

We further examined the capacity of the formed proteins to transport citrate across the plasma membrane by feeding them ^{13}C-labelled citrate and measuring the ^{13}C inside the cells with mass spectrometry. Citrate uptake ability was confirmed for the wild-type NaCT expressing cell lines (Inoue *et al.*, 2002) and was absent in all mutant cell lines. Whereas type I mutants were expected to have a quantitative loss of transporter function, a complete loss-of-function was also shown for type II mutants, despite correct protein folding and transport to the plasma membrane. A deficient sodium-binding site or disrupted substrate pocket is likely to account for this qualitative loss-of-function. Indeed, *in silico* modelling of type II mutations showed that both p.Thr142Met and p.Thr227Met are located at the citrate binding pocket (Fig. 4), most likely inducing a loss of citrate affinity. The p.Asp524His, on the contrary, is located in the last transmembrane domain and near the extracellular C-terminus. We hypothesize that this mutation might disrupt the conformational shift required for substrate translocation over the membrane (Mancusso *et al.*, 2012). All mutations result in a total loss-of-function of NaCT, which correlates with the fact that there does not seem to be an association between mutation type and seizure severity or cognitive outcome.

The *SLC13A* gene family encodes five sequence-related proteins that function as high-affinity sodium sulphate (NaS) or sodium carboxylate (NaC) co-transporters. Their crucial role in cell functionality is supported by the wide expression in various tissues and the existence of orthologues throughout evolution. The *SLC13A5* gene specifically encodes the sodium-citrate transporter NaCT and is mainly expressed in liver and brain (Bergeron *et al.*, 2013). The consequences of NaCT dysfunction in the liver have been studied in several (partial) knock-out animals: a reduced expression of NaCT orthologues promotes longevity, which is probably due to increased hepatic mitochondrial biogenesis (Rogina *et al.*, 2000; Fei *et al.*, 2003; Wada *et al.*, 2006; Birkenfeld *et al.*, 2011). None of these animals show evidence of epileptic activity or other neurological signs. The discrepancy between human and animal phenotypes can possibly be explained by the presence of species-specific compensatory mechanisms and differences in brain cellular expression of the NaC-transporter family (Wada *et al.*, 2006; Yodoya *et al.*, 2006; Birkenfeld *et al.*, 2011; Lamp *et al.*, 2011; Pajor, 2014). Unlike other cell types, neurons are incapable of *de novo* tricarboxylic acid (TCA) intermediate synthesis. Therefore they express high-affinity transporters such as NaCT to take up key metabolites including citrate, which are synthesized and released by neighbouring astrocytes (Sonnewald *et al.*, 1991; Rodrigues *et al.*, 2013). We showed that the epileptic encephalopathy-associated *SLC13A5* mutations cause a loss of citrate uptake capacity, however, the different TCA cycle machinery of non-neuronal cultures compared to neurons make HEK293T cells unsuitable to investigate the downstream effects of dysfunctional citrate anaplerosis. Based on the currently available data, we can nevertheless postulate

Table 2 Summary of molecular characterization of *SLC13A5* mutations

Cell line	Protein formation			Cellular localization		Transporter function
	Primary	Secondary	Aberrant	Plasma membrane	Intracellular	^{13}C-citrate uptake
WT	+ +	+	–	+ +	+	+
p.Ser427Leu	–	+ +	–	–	+ +	–
p.Trp341*	–	–	+	–	+ +	–
p.Pro407Argfs*12	–	–	+	–	+ +	–
p.Gly219Arg	–	+ +	–	–	+ +	–
p.Thr142Met	+	+	–	+ +	+	–
p.Thr227Met	+	+	–	+ +	+	–
p.Asp524His	+	+	–	+ +	+	–

HEK293T cells expressing the respective *SLC13A5* plasmids were studied *in vitro*, using selective western blot (protein formation) immunocytochemistry (cellular localization), and mass spectrometry (transporter function). The results are indicated with – = undetectable, + = detectable, and + + = highly detectable. Western blot (Fig. 3A) showed a specific band pattern for wild-type expressing cells: the observed primary and secondary band were detectable in different degrees for mutant expressing cells. The truncating mutations induced the formation of an aberrant protein. Immuncytochemistry (Fig. 3B) showed a predominant plasma membrane localization for wild-type and mutation type II expressing cells, whereas the proteins formed by mutation type I expressing cells resided in the endoplasmatic reticulum. Only wild-type expressing cells were able to transport a measurable amount of 13C-citrate over the plasma membrane.

three potential pathomechanisms underlying *SLC13A5* encephalopathy. To start, insufficient supply of TCA intermediates could result in brain energy failure, which is a known cause of epileptic encephalopathy [e.g. GLUT1 deficiency (MIM 614847) or early onset epileptic encephalopathy type 3 (MIM 609304)] and hints towards a favourable outcome of therapies that provide alternative sources for energy production such as the ketogenic diet (Roe and Mochel 2006; Willis *et al.*, 2010; Kim *et al.*, 2013). Interestingly, a positive effect of the ketogenic diet on seizure control and/or development was seen in the three patients who tried this treatment. Yet, it should be taken into account that despite the fact that the diet theoretically bypasses the normal route of brain energy supply, an effect through alternative anti-convulsive properties cannot be excluded (Hughes *et al.*, 2014). Larger prospective studies are needed to clarify whether NaCT-deficient patients would specifically benefit from starting the diet early in life, similar to what has been described for GLUT1-deficient patients (Brockmann, 2009; Hallbook *et al.*, 2012). Secondly, as a precursor of α-ketoglutarate, citrate can be used as substrate for glutamine and GABA production by metabolization through the TCA cycle (Schousboe *et al.*, 1997; Hertz and Zielke, 2004). An imbalanced neurotransmitter production is a well-known pathomechanism in epilepsy and more specifically epileptic encephalopathy (EuroEPINOMICS-RES Consortium *et al.*, 2014). One patient (Family A) had neurotransmitters measured in CSF during his diagnostic work-up, and values were within normal limits. The test was considered too invasive to be performed in the other patients purely for the purpose of this study. Lastly, due to accumulation of citrate in the extracellular environment, citrate can act as a zinc chelator and could indirectly attenuate *N*-methyl D-aspartate receptor inhibition (Sonnewald *et al.*, 1991; Westergaard *et al.*, 1995). As for its role in teeth development, citrate can also act as a magnesium and calcium chelator. Defects of ion channels and transporters involved in the regulation of calcium homeostasis are a well-known cause of teeth malformations (Duan, 2014). An important role for *SLC13A5* in teeth development is supported by a gene expression analysis, which showed *Slc13a5* to be one of the top 15 genes upregulated during mouse molar development (Pemberton *et al.*, 2007).

In conclusion, we provide independent evidence that autosomal recessive inherited mutations in *SLC13A5* lead to a severe neonatal epileptic encephalopathy with frequent status epilepticus at onset, and different degrees of developmental delay (MIM 615905). We also highlight that teeth hypoplasia or hypodontia is a clinically recognizable feature of *SLC13A5* encephalopathy, and should warrant *SLC13A5* screening. A complete loss of citrate transport for all *SLC13A5* mutations identified here was shown to be based on two different cellular mechanisms: (i) a quantitative loss of function due to lack of correct protein formation and plasma membrane localization; or (ii) a qualitative loss of function possibly due to a defected sodium-binding site, binding pocket or confirmation shift (overview in Table 2). Our study exemplifies the possible differential effect of individual mutations on a molecular level. Additional studies in a neuronal cell system or animal model are required to study the downstream effects of NaCT-deficiency in detail and investigate the involvement of neuronal energy supply, neurotransmitter production and modification of neuronal activity as potential pathomechanisms in *SLC13A5*-encephalopathy.

Acknowledgements

We thank the families and patients for their participation to this study. We also thank Michiel Krols, Vicky De Winter, Peter Van Hasselt, and Max Haesendonckx for assisting with the endoplasmic reticulum stress experiments, viral

work, metabolic screening and genetic follow-up respectively. The Family Genomics group at the Institute for Systems Biology deserves thanks for their support and project management of the whole-genome sequencing data. We acknowledge the contribution of Peter De Rijk (as developer of GenomeComb - Antwerp pipeline) and the HPC facilities of the University of Luxembourg (http://hpc.uni.lu) for computational support, the VIB Genetic Service Facility for the genetic follow-up analyses (http://www.vib-geneticservicefacility.be), and Prof. Els Prinsen for the TQD. Also thanks to Tim Willems from CeProMa (directed by Prof. Yves Guisez) for his technical assistance with the mass spectrometry.

Funding

Within the Eurocores program of the European Science Foundation P.D.J. (G.A.136.11.N and FWO/ESF-ECRP) and I.H. (HE5415/3-1) received financial support within the EuroEPINOMICS-RES network, and P.N. (Nu50/8-1) and H.L. (Le1030/11-1) within the EuroEPINOMICS-CoGIE network. This work was further supported by the University of Antwerp and the Fund for Scientific Research Flanders (FWO). K.H. is a PhD fellow of the Institute for Science and Technology (IWT)-Flanders and T.G. of the FWO; A.S. is a postdoctoral fellow of the FWO. P.M. is supported as a ISB/LCSB fellow by "le plan Technologies de la Santé par le Government du Grand-Duché de Luxembourg" through the Luxembourg Centre for Systems Biomedicine (LCSB) at the University of Luxembourg. B.P.C.K. and C.G.F.K. were supported by the Dutch Epilepsy Fund (grant 10-09). H.L. and P.N. received additional funding of the German Federal Ministry of Education and Research (BMBF: NGFNplus/EMINet 01GS08123 and 01GS08120, IonNeurONet 01GM1105).

Supplementary material

Supplementary material is available at *Brain* online.

References

Allen AS, Berkovic SF, Cossette P, Delanty N, Dlugos D, Eichler EE, et al. *De novo* mutations in epileptic encephalopathies. Nature 2013; 501: 217–21.

Berg AT, Berkovic SF, Brodie MJ, Buchhalter J, Cross JH, van Emde Boas W, et al. Revised terminology and concepts for organization of seizures and epilepsies: report of the ILAE Commission on Classification and Terminology, 2005-2009. Epilepsia 2010; 51: 676–85.

Bergeron MJ, Clemencon B, Hediger MA, Markovich D. SLC13 family of Na(+)-coupled di- and tri-carboxylate/sulfate transporters. Mol Aspects Med 2013; 34: 299–12.

Birkenfeld AL, Lee HY, Guebre-Egziabher F, Alves TC, Jurczak MJ, Jornayvaz FR, et al. Deletion of the mammalian INDY homolog mimics aspects of dietary restriction and protects against adiposity and insulin resistance in mice. Cell Metab 2011; 14: 184–95.

Claes L, Del-Favero J, Ceulemans B, Lagae L, Van BC, De JP. De novo mutations in the sodium-channel gene SCN1A cause severe myoclonic epilepsy of infancy. Am J Hum Genet 2001; 68: 1327–32.

Drmanac R, Sparks AB, Callow MJ, Halpern AL, Burns NL, Kermani BG, et al. Human genome sequencing using unchained base reads on self-assembling DNA nanoarrays. Science 2010; 327: 78–81.

Brockmann K. The expanding phenotype of GLUT1-deficiency syndrome. J Brain Dev 2009; 31: 545–52.

Duan X. Ion channels, channelopathies, and tooth formation. J Dent Res 2014; 93: 117–25.

EuroEPINOMICS-RES Consortium, Epilepsy Phenome/Genome Project, Epi4K Consortium. *De novo* mutations in synaptic transmission genes including dnm1 cause epileptic encephalopathies. Am J Hum Genet 2014; 95: 360–70.

Fei YJ, Inoue K, Ganapathy V. Structural and functional characteristics of two sodium-coupled dicarboxylate transporters (ceNaDC1 and ceNaDC2) from Caenorhabditis elegans and their relevance to life span. J Biol Chem 2003; 278: 6136–44.

Gennaro E, Santorelli FM, Bertini E, Buti D, Gaggero R, Gobbi G, et al. Somatic and germline mosaicisms in severe myoclonic epilepsy of infancy. Biochem Biophys Res Commun 2006; 341: 489–93.

Hallbook T, Ji S, Maudsley S, Martin B. The effects of the ketogenic diet on behavior and cognition. Epilepsy Res 2012; 100: 304–9.

Hardies K, May P, Djemie T, Tarta-Arsene O, Deconinck T, Craiu D, et al. Recessive loss-of-function mutations in AP4S1 cause mild fever-sensitive seizures, developmental delay and spastic paraplegia through loss of AP-4 complex assembly. Hum Mol Genet 2014; 24: 2218–27.

Hertz L, Zielke HR. Astrocytic control of glutamatergic activity: astrocytes as stars of the show. Trends Neurosci 2004; 27: 735–43.

Hughes SD, Kanabus M, Anderson G, Hargreaves IP, Rutherford T, O'Donnell M, et al. The ketogenic diet component decanoic acid increases mitochondrial citrate synthase and complex I activity in neuronal cells. J Neurochem 2014; 129: 426–33.

Inoue K, Zhuang L, Ganapathy V. Human Na+ -coupled citrate transporter: primary structure, genomic organization, and transport function. Biochem Biophys Res Commun 2002; 299: 465–71.

Kamentsky L, Jones TR, Fraser A, Bray MA, Logan DJ, Madden KL, et al. Improved structure, function and compatibility for CellProfiler: modular high-throughput image analysis software. Bioinformatics 2011; 27: 1179–80.

Kelley LA, Sternberg MJ. Protein structure prediction on the Web: a case study using the Phyre server. Nat Protoc 2009; 4: 363–71.

Kim TH, Borges K, Petrou S, Reid CA. Triheptanoin reduces seizure susceptibility in a syndrome-specific mouse model of generalized epilepsy. Epilepsy Res 2013; 103: 101–5.

Kramer U, Nevo Y, Neufeld MY, Fatal A, Leitner Y, Harel S. Epidemiology of epilepsy in childhood: a cohort of 440 consecutive patients. Pediatr Neurol 1998; 18: 46–50.

Lamp J, Keyser B, Koeller DM, Ullrich K, Braulke T, Muhlhausen C. Glutaric aciduria type 1 metabolites impair the succinate transport from astrocytic to neuronal cells. J Biol Chem 2011; 286: 17777–84.

Larkin MA, Blackshields G, Brown NP, Chenna R, McGettigan PA, McWilliam H, et al. Clustal W and clustal X version 2.0. Bioinformatics 2007; 23: 2947–8.

Lennon G, Auffray C, Polymeropoulos M, Soares MB. The I.M.A.G.E. Consortium: an integrated molecular analysis of genomes and their expression. Genomics 1996; 33: 151–2.

Li H, Durbin R. Fast and accurate short read alignment with Burrows-Wheeler transform. Bioinformatics 2009; 25: 1754–60.

Mancusso R, Gregorio GG, Liu Q, Wang DN. Structure and mechanism of a bacterial sodium-dependent dicarboxylate transporter. Nature 2012; 491: 622–6.

Mefford HC, Yendle SC, Hsu C, Cook J, Geraghty E, McMahon JM, et al. Rare copy number variants are an important cause of epileptic encephalopathies. Ann Neurol 2011; 70: 974–85.

Molinari F, Kaminska A, Fiermonte G, Boddaert N, Raas-Rothschild A, Plouin P, et al. Mutations in the mitochondrial glutamate carrier SLC25A22 in neonatal epileptic encephalopathy with suppression bursts. Clin Genet 2009; 76: 188–94.

Paciorkowski AR, Weisenberg J, Kelley JB, Spencer A, Tuttle E, Ghoneim D, et al. Autosomal recessive mutations in nuclear transport factor KPNA7 are associated with infantile spasms and cerebellar malformation. Eur J Hum Genet 2013; 22: 587–93.

Pajor AM. Sodium-coupled dicarboxylate and citrate transporters from the SLC13 family. Pflugers Arch 2014; 466: 119–30.

Panayiotopoulos CP. The epilepsies: seizures, syndromes and management, Chapter 7. Epileptic encephalopathies in infancy and early childhood in which the epileptiform abnormalities may contribute to progressive dysfunction. Oxfordshire: Bladon Medical Publishing; 2005. http://www.ncbi.nlm.nih.gov/books/NBK2611/

Pemberton TJ, Li FY, Oka S, Mendoza-Fandino GA, Hsu YH, Bringas P, Jr, et al. Identification of novel genes expressed during mouse tooth development by microarray gene expression analysis. Dev Dyn 2007; 236: 2245–57.

Reinthaler EM, Dejanovic B, Lal D, Semtner M, Merkler Y, Reinhold A, et al. Rare variants in gamma-aminobutyric acid type A receptor genes in rolandic epilepsy and related syndromes. Ann Neurol 2015; 6: 972–86.

Reumers J, De Rijk P, Zhao H, Liekens A, Smeets D, Cleary J, et al. Optimized filtering reduces the error rate in detecting genomic variants by short-read sequencing. Nat Biotechnol 2012; 30: 61–8.

Rodrigues TB, Valette J, Bouzier-Sore AK. (13)C NMR spectroscopy applications to brain energy metabolism. Front Neuroenerget 2013; 5: 9.

Roe CR, Mochel F. Anaplerotic diet therapy in inherited metabolic disease: therapeutic potential. J Inherit Metab Dis 2006; 29: 332–40.

Rogina B, Reenan RA, Nilsen SP, Helfand SL. Extended life-span conferred by cotransporter gene mutations in Drosophila. Science 2000; 290: 2137–40.

Schousboe A, Westergaard N, Waagepetersen HS, Larsson OM, Bakken IJ, Sonnewald U. Trafficking between glia and neurons of TCA cycle intermediates and related metabolites. Glia 1997; 21: 99–105.

Schubert J, Siekierska A, Langlois M, May P, Huneau C, Becker F, et al. Mutations in STX1B, encoding a presynaptic protein, cause fever-associated epilepsy syndromes. Nat Genet 2014; 46: 1327–32.

Sonnewald U, Westergaard N, Krane J, Unsgard G, Petersen SB, Schousboe A. First direct demonstration of preferential release of citrate from astrocytes using [13C]NMR spectroscopy of cultured neurons and astrocytes. Neurosci Lett 1991; 128: 235–9.

Thevenon J, Milh M, Feillet F, St-Onge J, Duffourd Y, Jugé C, et al. Mutations in SLC13A5 cause autosomal-recessive epileptic encephalopathy with seizure onset in the first days of life. Am J Hum Genet 2014; 95: 113–20.

Van Durme J, Delgado J, Stricher F, Serrano L, Schymkowitz J, Rousseau F. A graphical interface for the FoldX forcefield. Bioinformatics 2011; 27: 1711–12.

Vandesompele J, De PK, Pattyn F, Poppe B, Van Roy N, De Paepe A, et al. Accurate normalization of real-time quantitative RT-PCR data by geometric averaging of multiple internal control genes. Genome Biol 2002; 3: research0034.1–11

Veeramah KR, Johnstone L, Karafet TM, Wolf D, Sprissler R, Salogiannis J, et al. Exome sequencing reveals new causal mutations in children with epileptic encephalopathies. Epilepsia 2013; 54: 1270–81.

Wada M, Shimada A, Fujita T. Functional characterization of Na + -coupled citrate transporter NaC2/NaCT expressed in primary cultures of neurons from mouse cerebral cortex. Brain Res 2006; 1081: 92–100.

Weckhuysen S, Korff CM. Epilepsy: old syndromes, new genes. Curr Neurol Neurosci Rep 2014; 14: 447.

Westergaard N, Banke T, Wahl P, Sonnewald U, Schousboe A. Citrate modulates the regulation by Zn2 + of N-methyl-D-aspartate receptor-mediated channel current and neurotransmitter release. Proc Natl Acad Sci USA 1995; 92: 3367–70.

Willis S, Stoll J, Sweetman L, Borges K. Anticonvulsant effects of a triheptanoin diet in two mouse chronic seizure models. Neurobiol Dis 2010; 40: 565–72.

Yodoya E, Wada M, Shimada A, Katsukawa H, Okada N, Yamamoto A, et al. Functional and molecular identification of sodium-coupled dicarboxylate transporters in rat primary cultured cerebrocortical astrocytes and neurons. J Neurochem 2006; 97: 162–173.

Zheng L, Baumann U, Reymond JL. An efficient one-step site-directed and site-saturation mutagenesis protocol. Nucleic Acids Res 2004; 32: e115.

Appendix 1

Collection of samples was done within the autosomal recessive working group of the EuroEPINOMICS-RES consortium therefore we acknowledge the work of Zaid Afawi, Stéphanie Baulac, Hande Caglayan, Rosa Guerrero Lopez, Renzo Guerrini, Helle Hjalgrim, Johanna Jähn, Karl Martin Klein, Eric Leguern, Johannes Lemke, Carla Marini, Hiltrud Muhle, Felix Rosenow, Jose Serratosa, Katalin Štěrbová, Rikke S. Moller, Pasquale Striano, and Federico Zara.